A metamaterial-based interface for the structural resonance shielding of impact-driven offshore monopiles

Azevedo Vasconcelos, Ana Carolina; Valiya Valappil, Sabiju; Schott, Dingena; Jovanova, Jovana; Aragón, Alejandro M.

DOI
10.1016/j.engstruct.2023.117261

Publication date
2024

Document Version
Final published version

Published in
Engineering Structures

Engineering Structures 300 (2024) 117261

Contents lists available at ScienceDirect

Engineering Structures

journal homepage: www.elsevier.com/locate/engstruct

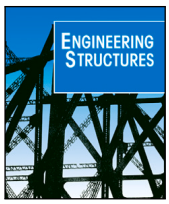

A metamaterial-based interface for the structural resonance shielding of impact-driven offshore monopiles

Ana Carolina Azevedo Vasconcelos, Sabiju Valiya Valappil, Dingena Schott, Jovana Jovanova, Alejandro M. Aragón *

Faculty of Mechanical Engineering, Delft University of Technology, Mekelweg 2, 2628 CD Delft, The Netherlands

ARTICLE INFO

Keywords:
Acoustic/elastic metamaterials
Noise attenuation
Resonance shielding
Single-phase unit cell

ABSTRACT

Underwater noise resulting from the monopile driving process can cause severe damage to marine wildlife, such as hearing injury, behavioral disturbance, or even death. Although current noise-attenuation techniques used in this process have shown a significant noise reduction at high frequency ranges, mitigating low-frequency noise is still extremely challenging. To address the problem, here we propose an elastic metamaterial-based structure composed of single-phase resonant structures. The proposed structure, which we call a meta-interface, is introduced between the monopile and the hammer and is used to remove energy from the input signal associated with high noise levels. To that end, we first identify the frequency ranges associated with high sound pressure levels, which were shown to be related to the monopile's eigenmodes. Then we design the meta-interface's periodic unit cells so that the elastic/acoustic waves at identified frequency ranges are attenuated. A meta-interface is then realized by replicating the unit cell along the monopile wall (matching the thickness) to form a ring-shaped layer, and then by stacking up these concentric layers. A frequency analysis of the pile driving system with the meta-interface shows that the new noise levels attain a significant attenuation in frequency ranges lower than 1000 Hz. This demonstrates a novel solution for the low-frequency underwater noise issue during the hammering of offshore monopiles.

1. Introduction

Most offshore wind turbines are installed on top of monopiles, which are the foundation of choice (80.5% in 2020) due to their straightforward manufacturing [1]. However, monopiles are driven into the ground by hammering, which results in sound pressure waves that propagate for distances in order of kilometers in seawater causing injuries to marine life [2–4]. To mitigate the high noise levels produced by monopile driving, several mechanisms have been proposed, such as enclosing the pile with casings [5], air-bubble curtains [6], and a combination of encapsulated bubbles with foam elements [7]. Such techniques have proven to be effective at reducing noise higher than 1 kHz. Bellmann [8] reported that the highest noise reduction, among all available noise mitigation systems, was achieved in the 1–2 kHz range. For the next generation of monopiles, high noise levels can be reached at lower frequencies as a consequence of the increasing average capacity of wind turbines—from 2018 to 2019, such capacity increased by 1 MW [1]. This is because larger monopiles are required to support the higher-capacity wind turbines, which incidentally shift the high-noise frequencies – associated to the monopile's eigenmodes – below 1 kHz. Since traditional noise mitigation techniques are not suited for frequencies below 1 kHz, several mechanisms need to be combined to reach the necessary noise reduction, which make it time consuming and operationally expensive. The IHC Noise Mitigation System (IHC-NMS), for instance, combines a double-wall steel pipe filled with air and a bubble curtain between the pile and the pipe walls, resulting in a noise reduction of about 7.5 dB at 800 Hz [5].

Acoustic/elastic metamaterials (A/E MMs), architected structures with unusual properties not commonly found in nature, have shown to be viable for low frequency noise mitigation [9,10]. The attenuation mechanism of A/E MMs originates from locally resonant structures [11]; these resonators produce resonant band gaps (BGs), which are frequency ranges where waves are attenuated due to the resonator's motion. A/E MMs can therefore realize subwavelength frequency attenuation—*i.e.*, the dimension of the periodic unit cell (PUC) can be orders of magnitude smaller than the target attenuated wavelength. The resonant effect of the first A/E MMs were initially attributed to the combination of materials with high impedance mismatch [12–14] and recently extended to single-material configurations, due to the advances of additive manufacturing processes and laser-cutting

* Corresponding author.
E-mail address: a.m.aragon@tudelft.nl (A.M. Aragón).

https://doi.org/10.1016/j.engstruct.2023.117261
Received 13 February 2023; Received in revised form 2 November 2023; Accepted 26 November 2023
Available online 5 December 2023

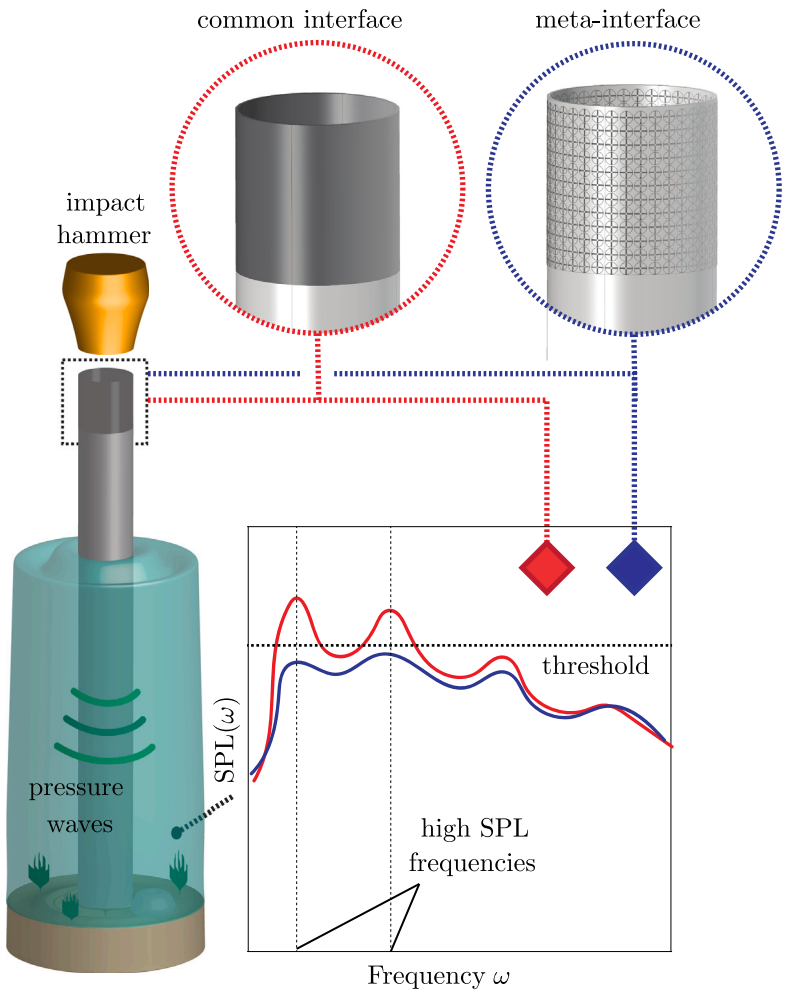

Fig. 1. Schematic representation of the meta-interface device for controlling wave propagation. The meta-interface, which is formed by periodic single-phase unit cells, transfers the impact's energy from the hammer to the monopile's head. The radial displacement of the monopile induces the propagation of pressure waves in water. The sound pressure level (SPL) is then calculated and compared with that from the common interface. The energy associated to high SPL (determined by the SPL threshold) is removed due to the functionality of the meta-interface.

techniques [15–20]. Although showing such intrinsic contributions in wave control, the potential of single-phase A/E MMs has not been fully explored in real-world problems, such as noise/vibration control in offshore environments, specially because of the time demanded to manufacture complex A/E MM designs for large-scale applications.

In this work we propose a novel single-phase A/E MM-based structure – called henceforth a meta-interface – which reduces the low-frequency underwater noise caused by the installation of offshore monopiles. Here we explore a single-phase unit cell with a planar geometry, so that straightforward manufacturing processes can be used. During the installation, the impact load's energy is transferred to the monopile through longitudinal waves [2]. Due to Poisson's effect, those waves induce radial displacements of the monopile, which produce a pressure field in water [21] (see Fig. 1). The meta-interface is then properly designed to selectively filter high-noise levels at specific frequencies – particularly, those related to the monopile's eigenmodes – so that the energy transmitted to the pile is enough to drive it into the ground. Frequency ranges causing high noise levels are identified via the analysis of the sound pressure level (SPL), which is a metric used by international regulations to quantify the sound levels in water [22]. Finally, the noise attenuation is compared to that of a standard cushion – also made of nylon – commonly used for controlling the amplitude and duration of the impact load, removing the stress concentrations on the pile head, and reducing the noise level [23]. Noteworthy, the focus of this work is on the noise reduction properties of the meta-interface. However, we also notice that the pulse used will undoubtedly result in high stresses within the meta-interface that can severely limit its functionality. Therefore, designing the meta-interface needs to account for mechanical performance and will be the subject of our future work. For sake of demonstration, here we design a meta-interface containing resonators with the same geometry, however, it is worth mentioning that multiple resonators with different ranges of attenuation could be used. This would allow us to control the amount of energy removed from the pile driving process. The proposed solution shows a significant attenuation of SPL at low-frequency ranges, which suggests its potential application in reducing the harmfulness in the underwater environment.

2. Methods

2.1. Dynamic characterization of meta-interface

The proposed meta-interface is composed by unit cells properly designed to filter energy from the impact load. To analyze the unit cell's dynamic characteristics, the band structure diagram is determined for wave vectors $\mathbf{k}$ varying through the boundaries of the irreducible Brillouin zone. For a periodic medium, the displacement field $\mathbf{u}$ satisfies

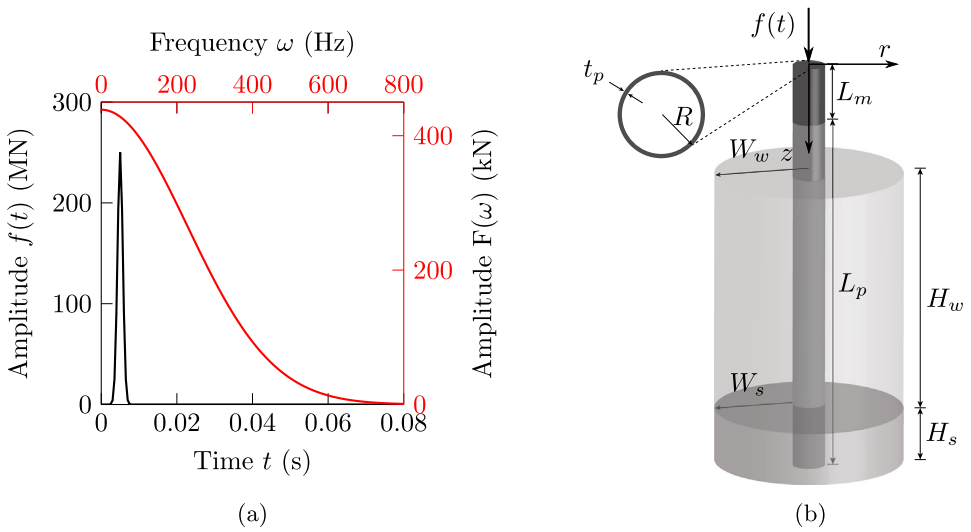

Fig. 2. (a) The impact load $f(t)$ applied on the top of the cushions is represented by a Gaussian pulse (in black) with corresponding frequency spectrum $\mathrm{F}(\omega)$ in red; (b) Geometric characterization of underwater sound prediction model. The darker gray cylinder represents the common cushion or the meta-interface. The geometric variables are presented in Table 1. (For interpretation of the references to color in this figure legend, the reader is referred to the web version of this article.)

the Bloch–Floquet theorem [24]

$$\mathbf{u}(\mathbf{r}) = \bar{\mathbf{u}}(\mathbf{r},\mathbf{k})\, e^{i(\mathbf{k}\cdot\mathbf{r})}, \tag{1}$$

where $\mathbf{r}$ is the position vector, $\bar{\mathbf{u}}(\mathbf{r},\mathbf{k})$ is a periodic displacement vector, and $i = \sqrt{-1}$. The finite element method (FEM) is used to define the eigenvalue problem, which is written as

$$[\mathbf{K}(\mathbf{k}) - \omega_n^2\mathbf{M}]\mathbf{u} = \mathbf{0}, \tag{2}$$

where $\mathbf{K}(\mathbf{k})$ and $\mathbf{M}$ are the stiffness and mass matrices, respectively; and the eigenvector $\mathbf{u}$ gives the motion of the unit cell's degrees of freedom related to the angular frequency ω_n. The band structure is then calculated by varying $\mathbf{k}$ along the IBZ's boundary and the resonant BGs are identified. In this study, a wavenumber sweep of $\Delta k = 0.001$ and a total of 30 eigenfrequencies were used to determine the band structure. The obtained eigenfrequencies $\omega = \omega(\mathbf{k})$ can be normalized as $\Omega = \omega a/c$, where c is the longitudinal wave speed of the constituent material and a is the unit cell size.

Since the band structure provides the dynamic characteristics for an infinite periodic medium, it is important to verify the wave mitigation in a finite domain. Thus, the transmission loss diagram is obtained by exciting the finite meta-interface with a harmonic input signal $\mathbf{U} = \bar{\mathbf{U}}\cos\omega t$, where $\bar{\mathbf{U}}$ is the displacement vector. The structure analyzed consists of an array of 14 unit cells, being $\mathbf{U}_1$ and $\mathbf{U}_2$ the displacements at points $\mathbf{x}_1$ (before) and $\mathbf{x}_2$ (after) the array, respectively. The input signal, which is applied perpendicularly along the top boundary of such array, consists of a prescribed displacement with an amplitude of 0.1 mm. Periodic boundary conditions are applied at the left and right boundaries. A PML is assumed at the bottom boundary to prevent the contribution of reflected waves on the displacement of the measure points. The input signal frequency is swept from 1 Hz to 1000 Hz with steps of 1 Hz. The frequency response is then evaluated by solving,

$$(\mathbf{K} - \omega^2\mathbf{M})\bar{\mathbf{U}} = \bar{\mathbf{F}}, \tag{3}$$

where $\bar{\mathbf{F}}$ denotes the amplitude vector of external harmonic forces ($\mathbf{F} = \bar{\mathbf{F}}\cos\omega t$). The transmission loss TL is defined as

$$\mathrm{TL\ (dB)} = 20\log_{10}\left(\frac{\|\mathbf{U}_2\|}{\|\mathbf{U}_1\|}\right). \tag{4}$$

2.2. Determination of the sound pressure level (SPL)

The SPL resulted from the pile driving process is calculated through three steps. Initially, the contact problem for the hammer strike is replaced by a compressive impact load applied at the top of the cushions. This assumption neglects the rebound effect of the hammer, which could induce a second impact load that may excite different pile modes and would require different resonator designs. However, the main part of the energy is transmitted to the pile through the first impact [25]. This is an assumption usually used by underwater noise prediction models and can give a good indication of the underwater noise spectrum. In the second step, the interaction between the impact load and the cushions are analyzed separately from the pile-soil–water system. Through a frequency domain analysis, the reaction force is determined at the bottom surface of both cushions. Finally, the reaction force is introduced as a boundary condition in the pile-water–soil model, from which the SPL is calculated in the frequency domain. More details about each step are given further.

The impact load applied is modeled as a symmetric vertical Gaussian pulse with amplitude 250 MN and a duration of 5 ms. It is worth emphasizing that these load's characteristics were selected so that a realistic representation of SPL is guaranteed. Its spectrum of excitation is determined by applying a fast Fourier transform (FFT), as shown in Fig. 2(a). Notice that the load energy is concentrated at frequencies lower than 800 Hz, which restricts the sound measurements to this frequency range. The load spectrum is then uniformly applied to the top of both cushions, whereas the pile interaction at their bottom boundary is replaced by an axial spring with stiffness $k_p = E_pA_p/L_p$, where E_p, A_p, and L_p are the Young's modulus, the cross-sectional area, and the length of the pile, respectively. Damping is considered in the cushions by applying an isotropic loss factor for Nylon of $\eta_n = 0.024$ [26]. A frequency domain analysis provides the reaction spectrum at the bottom of the cushions.

The reaction spectrum is then transferred to the pile-driving system – which describes the pile-soil–water interaction – as the new forcing function responsible for driving the monopile (See more details about the reaction spectra in Section SI2 of Supplementary Information). Since we assume that the impact load is symmetric, the pile-driving system is treated as a 2D axisymmetric model. For the monopile-water–soil system, a zero displacement is prescribed at the bottom of the monopile. The seasurface is modeled as a boundary with total pressure $p_t = 0$, while the lateral sea ends have a cylindrical radiation condition to eliminate wave reflections. Low-reflecting boundary conditions are also assumed at the external boundaries of the soil domain. Once the maximum frequency of the excitation spectrum F_{max} is determined – the energy's load is concentrated at frequencies below

Table 1
Geometric and material parameters of the pile-soil–water system. The subscripts p and s denote pressure (longitudinal) and shear wave speeds, respectively.

Pile	Value	Water	Value	Soil	Value
Length L_p (m)	55	Column height H_w (m)	45	Depth of layer H_s (m)	5
External radius R (m)	2.5	Column width W_w (m)	30	Soil width W_s (m)	30
Thickness t_p (mm)	90	PML width (m)	5	PML width (m)	5
Modulus E_p (GPa)	210	Density ρ_w (kg/m^3)	998	Density ρ_s (kg/m^3)	1600
Density ρ_p (kg/m^3)	7850	Wave speed c_p^w (m s^{-1})	1480	Wave speed c_p^s (m s^{-1})	1592
Poisson's ratio ν	0.28			Wave speed c_s^s (m s^{-1})	159

800 Hz – the minimum wavelength λ can be calculated through the expression $\lambda = c_{min}/F_{max}$, where c_{min} is the minimum wave speed of a specific domain. Therefore, the wavelengths in water and soil are $\lambda_w = 1.85$ m and $\lambda_s = 0.19$ m, respectively. A minimum of five finite elements per wavelength is considered in the model, which provides a minimum element size of 0.37 m for water and 0.04 m for soil. A frequency domain linear analysis of a structural-acoustic finite element model is then performed to predict SPLs at the underwater environment [2,27].

To quantify the noise propagation in the water, the SPL is measured at different locations. The SPL, in dB, is calculated as [28]

$$\mathrm{SPL}(\omega) = 20\log_{10}\left(\frac{\sqrt{2}}{2}\frac{|\bar{p}_t(r,z,\omega)|}{p_r}\right), \tag{5}$$

where r and z are the coordinates of the measurement points, $\bar{p}_t$ is the total pressure in the frequency domain and p_r is the reference pressure, which for water is $p_r = 1$ μPa. Since the modeled water domain has finite extension, an exterior field calculation by means of the Helmholtz–Kirchhoff integral [29] is set up to obtain the SPL at the distance defined by German regulations (190 dB at 750 m) based on the pressure and its normal derivative at the external underwater boundaries.

3. Results and discussion

3.1. Critical sound pressure levels

Fig. 2(b) describes the model used to predict the underwater noise that results from the pile driving process. The monopile is represented by a cylindrical shell made of steel, whereas the common interface, which represents a cushion commonly used, is placed on top. The diameter and thickness of the interface are equal to those of the monopile, and its length is $L_m = 5$ m. The material used for the interface is Nylon, with Young's modulus $E = 2$ GPa, mass density $\rho = 1150$ kg/m^3, and Poisson's ratio $\nu = 0.4$. The water column is mathematically described by an acoustic semi-infinite medium, in which perfectly matched layers (PMLs) are used to avoid wave reflections and the total pressure at the sea surface is $p_t = 0$. A semi-infinite elastic continuum is used to represent the soil. PMLs are also assumed at the soil's lateral and bottom surfaces. The geometric and material properties of the pile-water–soil system are given in Table 1. Finally, the hammer's loading is represented by a Gaussian impulse (see Fig. 2(a)) and is prescribed as a natural boundary condition applied at the top of the common interface. The steps described in Section 2.2 are then followed to determine the SPLs.

Several international regulations have defined the SPL threshold according to the species living in the environment, the distance to the noise source, the number of hammer blows, among other factors. From those regulations, the German one defined a maximum SPL of 190 dB at 750 m from the pile [22]. Fig. 3 summarizes the SPL response of the model at a point located 25 m above the seabed and 750 m away from the pile wall. To identify the frequency ranges that correspond to high sound pressure levels, the sound threshold is also drawn in the figure. Since the water domain considered here is finite, the external pressure field is calculated by means of the Helmholtz-Kirchhoff integral (see Section 2.2 in Methods). The inset in Fig. 3 highlights the peak at which the sound level is higher than the threshold. From an eigenfrequency analysis of a clamped monopile, the first five natural frequencies are calculated and marked in Fig. 3 with vertical lines. Their values are $f_1 = 22.955$ Hz, $f_2 = 68.739$ Hz, $f_3 = 114.1$ Hz, $f_4 = 158.58$ Hz, and $f_5 = 201.29$ Hz. It is worth noting that these frequencies correspond to some SPL peaks. More specifically, the highest SPL occurs near the frequency associated to the fifth monopile eigenmode f_5. For the remaining eigenfrequencies, we observe a relation between their values and some lower-amplitude peaks. Such relation occurs due to the coupling between the radial displacement of the monopile and the water particle motion [2,3,23]. During the hammer impact, a radial expansion/compression of the monopile undergoes as a result of the Poisson effect. The energy associated to this motion is then transferred to the surrounding water, which consequently causes the high SPL. Based on this analysis, the unit cell is designed to realize a resonant BG at the frequency range corresponding to the highest SPL.

3.2. Meta-interface design

In order to design the meta-interface, we first look at the single-phase periodic unit cell, which consists of a cylindrical mass of radius R_2 connected to an external frame with squared-size a (and cavity's radius R_1) through four identical beams of length l_b and width w_b, as shown in Fig. 4. The beam's paths have width w_g and depth l_g. Finally, the unit cell has a uniform thickness h. These parameters were tuned to create a resonant BG that falls in the frequency range corresponding to the highest SPL. Now that the PUC is defined, the meta-interface is realized by replacing it concentrically (with respect to the monopile's center), and then each layer is replicated vertically 12 times.

The single-phase unit cell presented in Fig. 4 has dimensions $a = 0.4$ m, $R_1 = 0.42a$, $R_2 = 0.365a$, $w_b = 0.02a$, $l_b = 0.99a$, $l_g = R_2 - 0.08a$, $w_g = 0.05a$, and $h = 0.225a$. Such dimensions were determined through a parametric study (See Section SI1 of Supplementary Information). The numerical characterization is conducted by obtaining the dispersion relation (band structure) and transmissibility analysis. While the former can be used to reveal band gaps by assuming an infinite metamaterial (which is done by enforcing Bloch–Floquet periodic conditions), the latter is used to obtain the actual attenuation of a finite-dimensional structure. Notice that the 8-fold symmetry of the unit cell requires its dispersion evaluation along the boundaries Γ-X-M-Γ of the Irreducible Brillouin Zone (IBZ) defined by the yellow triangle. Fig. 4 reveals a complete resonant BG at a frequency range extending from 196.69 Hz to 205.54 Hz (gray area). This means that waves with wavelength associated to the complete BG are attenuated, regardless of their direction of propagation. In the transmission loss diagram, a second peak at a frequency of 388.77 Hz is also observed, which is attributed to the resonant mode of the unit cell (indicated by M_2) and to the presence of a negative group velocity (negative slope of the dispersion curve), indicating a negative refraction index [30] in the $\Gamma - X$ direction (direction of the impact load). Another observation is that the wavelength associated to both frequency ranges is much longer than the dimensions of the unit cell, which characterizes subwavelength frequency attenuation. Finally, the asymmetric transmission loss observed along the BG frequency ranges also demonstrates resonant-type BGs.

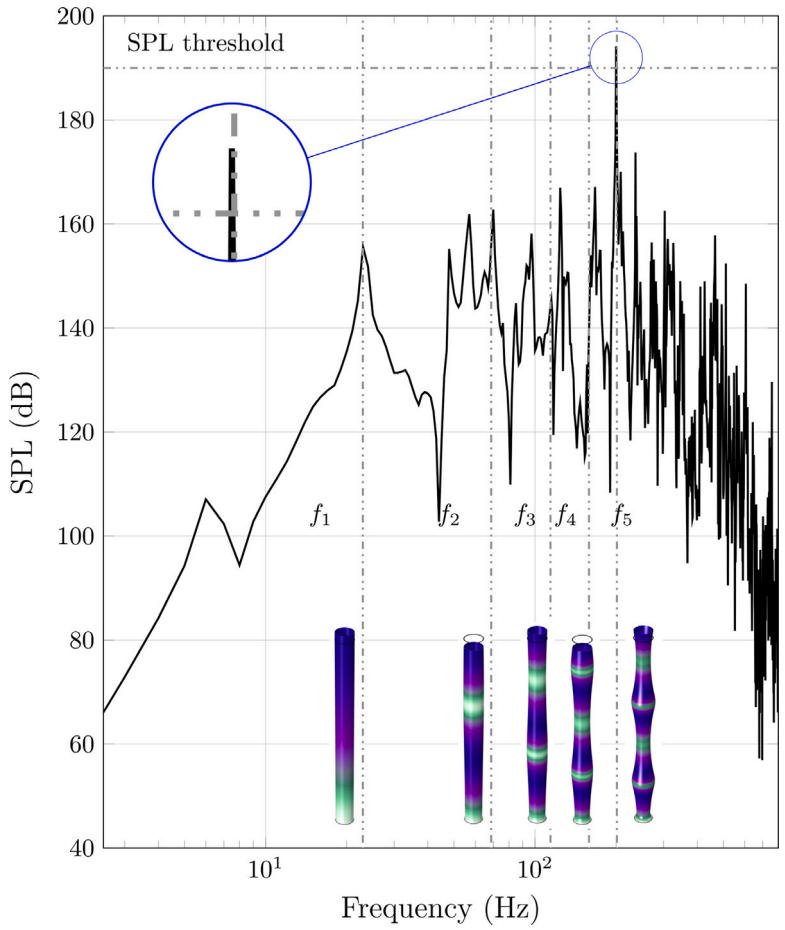

Fig. 3. Sound pressure level in the water domain that results from the hammer's impact. The measuring point is located at 25 m above the seabed and 750 m away from the monopile wall. Vertical lines indicate the monopile's first five eigenmode frequencies. The peak above 190 dB (SPL threshold) is located near the fifth monopile eigenfrequency (f_5 = 201.29 Hz).

3.3. Underwater noise reduction

To ensure that the SPL analyses (Section 2.2 of Methods) in a pile system containing a common cushion and a meta-interface are comparable, their heights are kept the same, (thus, the meta-interface possesses 12 ring-shaped layers; each layer contains 36 unit cells), as well as, the impact load (see Fig. 2(a)). Fig. 5 summarizes the results of this comparison. A reduction of approximately 98 dB is observed at the critical noise region. Such reduction is more than enough to guarantee that SPL for this frequency range is kept below 190 dB. As discussed in Section 3.2, the wave attenuation at such frequency range arises from the complete band gap. For more details about such discussion, please refer to Section SI3 of Supplementary Information. Other noise reduction behavior is observed at frequency around 382.77 Hz. For such case, a noise gap of 34 dB is obtained due to the presence of a locally resonant bandgap as shown in Fig. 4. It is important to notice that SPL associated to bands below 20 Hz are almost kept unchanged, which means that the energy associated to those bands is transmitted to the pile unaltered. At frequencies between 20 Hz and 40 Hz, we observe an increase in SPL due to the excitation of the meta-interface's natural frequencies (see Section SI2 of Supplementary Information). Although only the measurement at the middle of the underwater column is shown here, we observed a similar behavior at different underwater heights and close to the monopile (see Section SI4).

Fig. 5 shows that the SPL drops drastically at the band gaps (i.e, at SPLs much lower than the threshold), which implies that less energy is transmitted to the pile. The advantage of our system is that the transmitted energy can also be controlled by adding or removing unit cell layers—the minimum number of layers is chosen based on the minimum attenuation required to reach the sound pressure level threshold.

4. Conclusions

This work demonstrated numerically a meta-interface – a metamaterial-based structure composed of single-phase unit cells – for shielding the structural resonance of an offshore monopile to reduce the high underwater low-frequency noise levels. The periodic unit cell's resonator was designed according to critical frequency ranges causing high noise levels, which were shown to be associated to the natural frequencies of the monopile. The dynamic characteristics of the single-phase unit cells were analyzed via the dispersion relation and the transmission loss, which have identified a resonant BG corresponding to the critical frequency range. Such intrinsic features lead to a list of advantages of the presented noise mitigation approach. Compared with the common cushion, the proposed meta-interface guarantees a noise attenuation at the critical frequency range. Even though the inclusion of more unit cells allows us to obtain higher attenuation, the aim of the meta-interface is to remove energy from the impact load to a point that the SPL keeps acceptable levels and enough energy is transmitted to drive the monopile. Regarding the manufacturing process, the single-phase unit cell offers advantages for straightforward fabrication, which can be performed not only via 3D-printing but also with cutting techniques, such as laser cutting machines. Finally, the sound control is performed directly at the source, unlike traditional noise-reduction techniques that attempt at mitigating noise away from

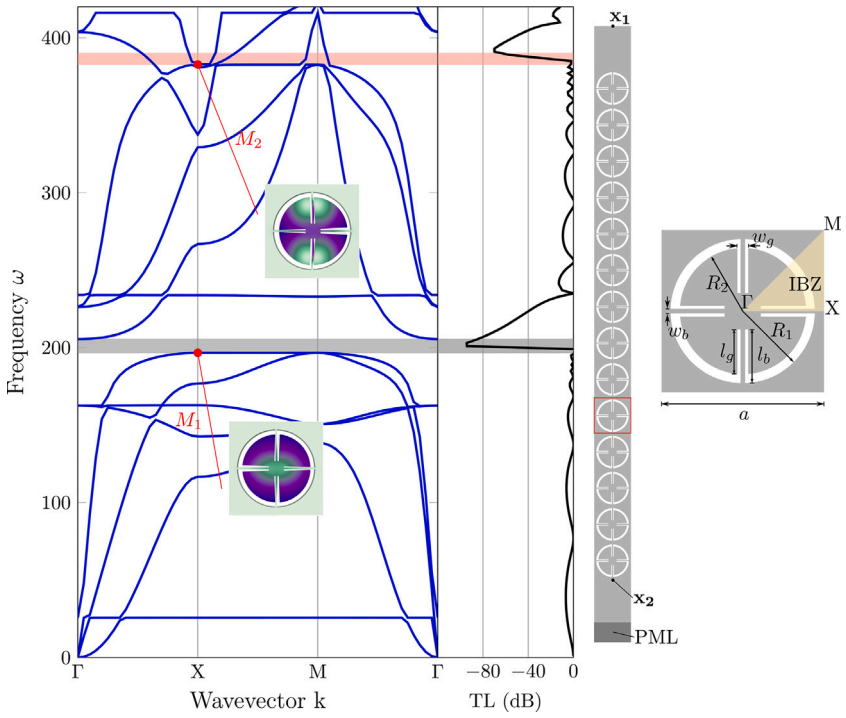

Fig. 4. Band structure of a periodic unit cell (PUC)—with an Irreducible Brillouin Zone (IBZ) defined in the yellow triangle, whose boundaries are given by the path Γ-X-M-Γ—and transmission loss diagrams for an array composed by 14 PUCs. The gray area identifies a complete BG with range $\omega = [196.69\,\text{Hz}, 205.54\,\text{Hz}]$. A partial BG is also identified at a frequency around 382.77 Hz (salmon area). The inset in the band structure diagram highlights the eigenmodes at the frequencies defining the band gaps in the Γ-X direction. In the vibration modes, the amplitude of displacement is indicated by the colormap from light green (minimum) to dark purple (maximum). (For interpretation of the references to color in this figure legend, the reader is referred to the web version of this article.)

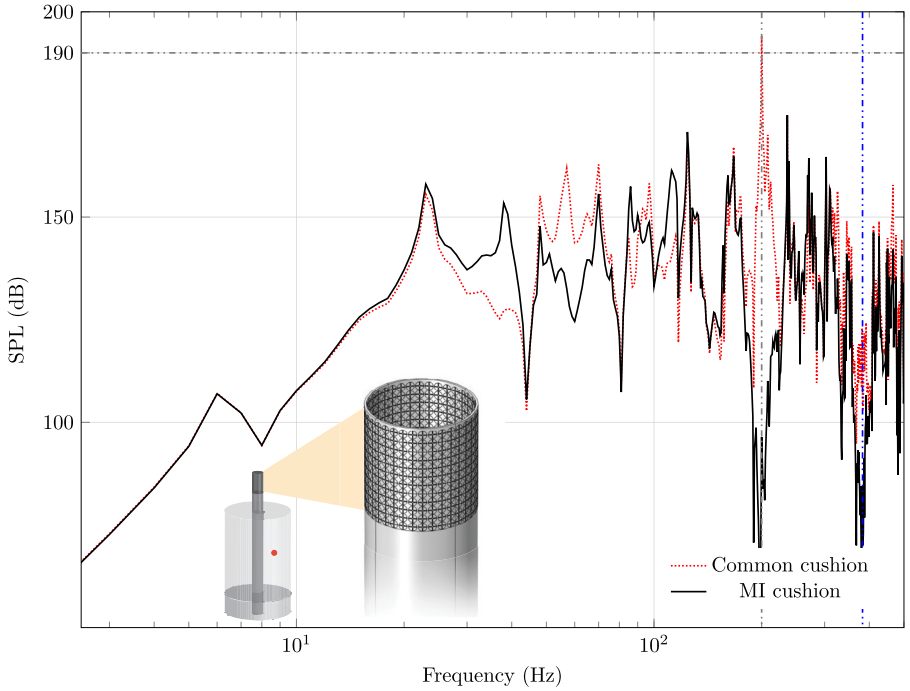

Fig. 5. SPL comparison between the common cushion (red dotted curve) and the meta-interface (solid black curve) at the measuring point shown in Fig. 3. The meta-interface contains 12 layers of periodically distributed unit cells; each layer has 36 unit cells at the radial direction. The SPL threshold is highlighted by the dashed horizontal line. The gray vertical lines indicate the frequencies where the noise reduction was obtained by the local resonance of the meta-interface. A reduction of 98 dB is observed in the region with the highest SPL, which occurs around 200 Hz (first vertical dashed line). (For interpretation of the references to color in this figure legend, the reader is referred to the web version of this article.)

the impact loading. Mitigating sound waves at their origin then avoids the use of huge structures that are used to encase the monopile, which further reduces costs and installation complexity and time.

Although the meta-interface concept predicts numerically the noise reduction during the pile installation, further studies are required to mature the concept. It is worth noting that the meta-interface design shown was tailored for a monopile with specific dimensions; therefore, changing the monopiles dimensions – thickness, diameter, or length – would require a completely different PUC design for attenuating different high noise levels effectively. Trial-and-error approaches for designing unit cells with specific attenuation properties is not straightforward, leading to the development of new design strategies, such as gradient-based optimization procedures [31], evolutionary algorithms [32], and inverse design by means of machine learning techniques [33]. Due to its local resonant nature, the meta-interface's band gap covers a narrow bandwidth, which may result in efficiency loss in the presence of manufacturing imperfections. To avoid this, a precise manufacturing of the resonator should be guaranteed. It is also important to highlight that other pile driving processes may generate noise with wider noise bands. Some works have proposed strategies to increase the attenuation band—for instance, by using MMs formed by multi-resonators [33–35], which could be well implemented in the presented unit cell design. Regarding the design, it is worth noting that computational techniques such as topology optimization can be used to create robust designs to manufacturing variability [34,35]. In addition, the mechanical integrity of the meta-interface needs to be considered early in the design process, since it is also necessary to withstand repeated impact loads. In subsequent research, we will explore a multi-objective optimization approach aimed at deriving unit cell geometries that can withstand high impact loads while preserving their attenuation characteristics within specified frequency ranges. The investigation will focus on combining these optimal geometries to broaden the attenuation band. Finally, an experimental validation is essential to demonstrate the effectiveness and applicability of the meta-interface in reducing SPL. Addressing such tasks might enable the potential use of meta-interfaces as a new mitigation noise technique, which will greatly improve the installation process of offshore monopiles.

CRediT authorship contribution statement

Ana Carolina Azevedo Vasconcelos: Conceptualization, Methodology, Writing – original draft. **Sabiju Valiya Valappil:** Methodology, Writing – review & editing. **Dingena Schott:** Project administration, Supervision, Writing – review & editing. **Jovana Jovanova:** Conceptualization, Funding acquisition, Project administration, Supervision, Writing – review & editing. **Alejandro M. Aragón:** Conceptualization, Funding acquisition, Project administration, Supervision, Writing – review & editing.

Declaration of competing interest

The authors declare the following financial interests/personal relationships which may be considered as potential competing interests: Alejandro Marcos Aragón has patent #P35203NL00/NBL pending to Delft University of Technology. The inventors of this patent are AC Azevedo Vasconcelos, J Jovanova, and AM Aragon.

Data availability

Data will be made available on request.

Acknowledgment

This research was funded through a cohesion grant of the Faculty of Mechanical Engineering at Delft University of Technology.

Appendix A. Supplementary data

Supplementary material related to this article can be found online at https://doi.org/10.1016/j.engstruct.2023.117261.

References

[1] Ramirez Lizer, Fraile Daniel, Brindley G. Offshore wind in europe: Key trends and statistics 2019. 2020.
[2] Reinhall Per G, Dahl Peter H. Underwater mach wave radiation from impact pile driving: Theory and observation. J Acoust Soc Am 2011;130(3):1209–16.
[3] Dahl Peter H, de Jong Christ AF, Popper Arthur N. The underwater sound field from impact pile driving and its potential effects on marine life. Acoust Today 2015;11(2):18–25.
[4] Solé Marta, Sigray Peter, Lenoir Marc, van der Schaar Mike, Lalander Emilia, André Michel. Offshore exposure experiments on cuttlefish indicate received sound pressure and particle motion levels associated with acoustic trauma. Sci Rep 2017;7(1):1–13.
[5] Koschinski Sven, Lüdemann K. Development of noise mitigation measures in offshore wind farm construction. Comm Fed Agency Nat Conserv 2013;1–102.
[6] Bohne Tobias, Grießmann Tanja, Rolfes Raimund. Modeling the noise mitigation of a bubble curtain. J Acoust Soc Am 2019;146(4):2212–23.
[7] Elmer Karl-Heinz. Effective offshore piling noise mitigation in deep waters. J Civ Eng Archit 2018;12:662–8.
[8] Bellmann Michael A. Overview of existing noise mitigation systems for reducing pile-driving noise. In: Proceeding auf der internoise. 2014.
[9] Krushynska Anastasiia O, Bosia Federico, Pugno Nicola M. Labyrinthine acoustic metamaterials with space-coiling channels for low-frequency sound control. Acta Acust United Acust 2018;104(2):200–10.
[10] Gao Nansha, Wei Zhengyu, Zhang Ruihao, Hou Hong. Low-frequency elastic wave attenuation in a composite acoustic black hole beam. Appl Acoust 2019;154:68–76.
[11] Liu Zhengyou, Zhang Xixiang, Mao Yiwei, Zhu YY, Yang Zhiyu, Chan Che Ting, Sheng Ping. Locally resonant sonic materials. Science 2000;289(5485):1734–6.
[12] Tan Kwek Tze, Huang HH, Sun CT. Optimizing the band gap of effective mass negativity in acoustic metamaterials. Appl Phys Lett 2012;101(24):241902.
[13] Alamri Sagr, Li Bing, Tan KT. Dynamic load mitigation using dissipative elastic metamaterials with multiple maxwell-type oscillators. J Appl Phys 2018;123(9):095111.
[14] Hu Guobiao, Tang Lihua, Xu Jiawen, Lan Chunbo, Das Raj. Metamaterial with local resonators coupled by negative stiffness springs for enhanced vibration suppression. J Appl Mech 2019;86(8):081009.
[15] Elmadih W, Chronopoulos D, Syam WP, Maskery I, Meng Han, Leach RK. Three-dimensional resonating metamaterials for low-frequency vibration attenuation. Sci Rep 2019;9(1):1–8.
[16] Jiang Weifeng, Yin Ming, Liao Qihao, Xie Luofeng, Yin Guofu. Three-dimensional single-phase elastic metamaterial for low-frequency and broadband vibration mitigation. Int J Mech Sci 2021;190:106023.
[17] D'Alessandro Luca, Krushynska Anastasiia O, Ardito Raffaele, Pugno Nicola M, Corigliano Alberto. A design strategy to match the band gap of periodic and aperiodic metamaterials. Sci Rep 2020;10(1):1–13.
[18] Colombi Andrea, Colquitt Daniel, Roux Philippe, Guenneau Sebastien, Craster Richard V. A seismic metamaterial: The resonant metawedge. Sci Rep 2016;6(1):1–6.
[19] Du Qiujiao, Zeng Yi, Xu Yang, Yang Hongwu, Zeng Zuoxun. H-fractal seismic metamaterial with broadband low-frequency bandgaps. J Phys D: Appl Phys 2018;51(10):105104.
[20] Liu Ze, Dong Hao-Wen, Yu Gui-Lan, Cheng Li. Achieving ultra-broadband and ultra-low-frequency surface wave bandgaps in seismic metamaterials through topology optimization. Compos Struct 2022;115863.
[21] Jensen Finn B, Kuperman William A, Porter Michael B, Schmidt Henrik. Computational ocean acoustics. Springer Science & Business Media; 2011.
[22] Andersson Mathias H, Andersson Brodd Leif, Pihl Jörgen, Persson Leif KG, Sigray Peter, Andersson Sandra, Wikström Andreas, Ahlsén Jimmy, Hammar Jonatan. A framework for regulating underwater noise during pile driving. 2017.
[23] Deng Qingpeng, Jiang Weikang, Zhang Wenzheng. Theoretical investigation of the effects of the cushion on reducing underwater noise from offshore pile driving. J Acoust Soc Am 2016;140(4):2780–93.
[24] Hussein Mahmoud I, Leamy Michael J, Ruzzene Massimo. Dynamics of phononic materials and structures: Historical origins, recent progress, and future outlook. Appl Mech Rev 2014;66(4).
[25] Fricke Moritz B, Rolfes Raimund. Towards a complete physically based forecast model for underwater noise related to impact pile driving. J Acoust Soc Am 2015;137(3):1564–75.
[26] Dashtkar Arash, Hadavinia Homayoun, Barros-Rodriguez Jose, Williams Neil A, Turner Matthew, Vahid Samireh. Quantifying damping coefficient and attenuation at different frequencies for graphene modified polyurethane by drop ball test. Polym Test 2021;100:107267.

[27] Zampolli Mario, Nijhof Marten JJ, de Jong Christ AF, Ainslie Michael A, Jansen Erwin HW, Quesson Benoit AJ. Validation of finite element computations for the quantitative prediction of underwater noise from impact pile driving. J Acoust Soc Am 2013;133(1):72–81.

[28] Long Marshall. 2 - fundamentals of acoustics. In: Long Marshall, editor. Architectural acoustics (second edition). second ed.. Boston: Academic Press; 2014, p. 39–79.

[29] Ginsberg Jerry H. Acoustics: A textbook for engineers and physicists. vol. 2, Springer; 2018.

[30] Oh Joo Hwan, Kwon Young Eui, Lee Hyung Jin, Kim Yoon Young. Elastic metamaterials for independent realization of negativity in density and stiffness. Sci Rep 2016;6(1):23630.

[31] Lu Lirong, Yamamoto Takashi, Otomori Masaki, Yamada Takayuki, Izui Kazuhiro, Nishiwaki Shinji. Topology optimization of an acoustic metamaterial with negative bulk modulus using local resonance. Finite Elem Anal Des 2013;72:1–12.

[32] Dong Hao-Wen, Zhao Sheng-Dong, Wang Yue-Sheng, Zhang Chuanzeng. Topology optimization of anisotropic broadband double-negative elastic metamaterials. J Mech Phys Solids 2017;105:54–80.

[33] Bastek Jan-Hendrik, Kumar Siddhant, Telgen Bastian, Glaesener Raphaël N, Kochmann Dennis M. Inverting the structure–property map of truss metamaterials by deep learning. Proc Natl Acad Sci 2022;119(1):e2111505119.

[34] Halkjær Søren, Sigmund Ole, Jensen Jakob S. Maximizing band gaps in plate structures. Struct Multidiscip Optim 2006;32:263–75.

[35] Oh Joo Hwan, Ahn Young Kwan, Kim Yoon Young. Maximization of operating frequency ranges of hyperbolic elastic metamaterials by topology optimization. Struct Multidiscip Optim 2015;52:1023–40.